INTERFACE

royalsocietypublishing.org/journal/rsif

Research

Cite this article: Pepper RE, Riley EE, Baron M, Hurot T, Nielsen LT, Koehl MAR, Kiørboe T, Andersen A. 2021 The effect of external flow on the feeding currents of sessile microorganisms. *J. R. Soc. Interface* **18**: 20200953.
https://doi.org/10.1098/rsif.2020.0953

Received: 24 November 2020
Accepted: 1 February 2021

Subject Category:
Life Sciences–Physics interface

Subject Areas:
biophysics, biomechanics

Keywords:
environmental flows, *Vorticella*, sessile suspension feeders, recirculation, low Reynolds number, feeding currents

Author for correspondence:
Rachel E. Pepper
e-mail: rpepper@pugetsound.edu

Electronic supplementary material is available online at https://doi.org/10.6084/m9.figshare.c.5305463.

THE ROYAL SOCIETY PUBLISHING

The effect of external flow on the feeding currents of sessile microorganisms

Rachel E. Pepper[1], Emily E. Riley[2], Matthieu Baron[3], Thomas Hurot[4,5], Lasse Tor Nielsen[2], M. A. R. Koehl[6], Thomas Kiørboe[2] and Anders Andersen[2,5]

[1]Department of Physics, University of Puget Sound, Tacoma, WA 98416, USA
[2]Centre for Ocean Life, National Institute of Aquatic Resources, Technical University of Denmark, DK-2800 Kgs. Lyngby, Denmark
[3]École Normale Supérieure Paris-Saclay, 94230 Cachan, France
[4]École Polytechnique, 91128 Palaiseau, France
[5]Department of Physics, Technical University of Denmark, DK-2800 Kgs. Lyngby, Denmark
[6]Department of Integrative Biology, University of California Berkeley, Berkeley, CA 94720, USA

REP, 0000-0001-6804-8965; TK, 0000-0002-3265-336X; AA, 0000-0002-3831-1707

Microscopic sessile suspension feeders live attached to surfaces and, by consuming bacteria-sized prey and by being consumed, they form an important part of aquatic ecosystems. Their environmental impact is mediated by their feeding rate, which depends on a self-generated feeding current. The feeding rate has been hypothesized to be limited by recirculating eddies that cause the organisms to feed from water that is depleted of food particles. However, those results considered organisms in still water, while ambient flow is often present in their natural habitats. We show, using a point-force model, that even very slow ambient flow, with speed several orders of magnitude less than that of the self-generated feeding current, is sufficient to disrupt the eddies around perpendicular suspension feeders, providing a constant supply of food-rich water. However, the feeding rate decreases in external flow at a range of non-perpendicular orientations due to the formation of recirculation structures not seen in still water. We quantify the feeding flow and observe such recirculation experimentally for the suspension feeder *Vorticella convallaria* in external flows typical of streams and rivers.

1. Introduction

Microscopic sessile suspension feeders (MSSFs) are ubiquitous in marine and freshwater environments, including marine snow, biofilms and living hosts [1–5]. These single-celled protists typically have cell diameters in the range 5–100 µm and feed while attached to surfaces (figure 1*a*). MSSFs play a critical role in aquatic ecosystems because they are often the dominant predators of bacteria and phytoplankton, and serve as a critical food source for larger zooplankton [7–12]. MSSFs also improve the efficiency of wastewater treatment plants and may play a critical role in bio-remediation after human-caused disasters such as oil leaks, heavy metal contamination and sewage spills [13–17].

MSSFs generate a feeding current to draw in food. The feeding current determines their clearance rate (the volume of food-rich water processed per time) and feeding rate (amount of food consumed per time). The feeding current is generated either by a single flagellum, e.g. for choanoflagellates and other heterotrophic nanoflagllates, or by cilia, e.g. for ciliates like *Vorticella*, *Stentor* and *Opercularia*. Because these organisms live at low Reynolds number where viscous forces are dominant, the feeding current is strongly influenced by nearby boundaries, particularly the attachment surface. The proximity to this surface causes toroidal eddies in the feeding current that reduce clearance rates as water recirculates past the feeding apparatus [6,18–22].

MSSF orientation relative to the attachment surface strongly influences the extent to which recirculation occurs [6,19]. In still water, eddies in feeding currents for MSSFs oriented perpendicular to the attachment surface reduce

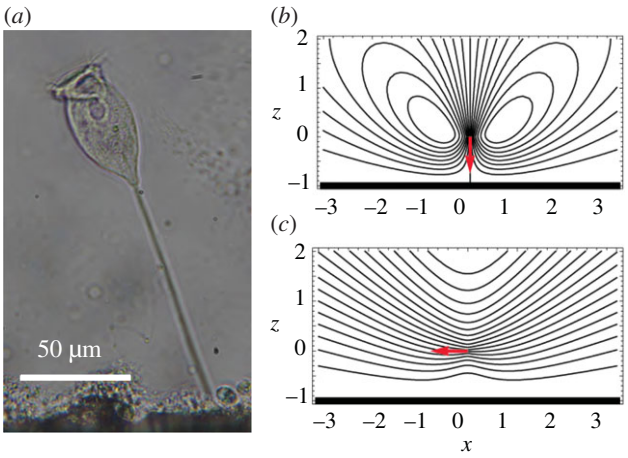

Figure 1. (*a*) Microscope image of *Vorticella*, a single-celled protist abundant in freshwater and marine environments. (*b*,*c*) Calculated streamlines for a model MSSF with no ambient flow (see [6] for details). The surface of attachment is the bold line, and the red arrow indicates the direction that the organism pushes the fluid. Streamlines show recirculation for organisms that feed perpendicular (*b*), and no recirculation when the force is parallel to the boundary (*c*).

clearance rates to zero over time (figure 1*b*), while no recirculation is present for MSSFs pushing parallel (figure 1*c*) and clearance rates are constant [6]. Recirculation times vary significantly among streamlines in the perpendicular case, and they can be of the order of minutes to several hours for the streamlines that pass close to the organism [6,23]. This means that, in some circumstances, diffusion of their food or motion of the organism can mitigate the effects of recirculation on the clearance rate [6,11,23].

These previous results focused on organisms in still water [6,19–23]. However, most MSSFs live in habitats with ambient flow that ranges from mm s^{-1} to m s^{-1} (table 1). Even in the viscous boundary layer near surfaces, where these organisms live, the flow is non-zero and may be enough to disrupt recirculation and increase food uptake [26].

Studies of the effect of flow on larger surface-attached organisms show that clearance rate generally increases with flow speed, but decreases at very high speeds [30–32]. Similar results have been found for a few species of MSSFs, but the effect of flow is strongly species dependent, and the mechanisms responsible have not been studied [33]. There is also indication that ambient flow can reduce or eliminate the eddies in the feeding current around perpendicular feeders, but there is no systematic study of this effect [34].

Here, we use experiments and calculations to gain a mechanistic understanding of how ambient flow affects MSSFs. We measure feeding flows and cell body orientations for the ciliate *Vorticella convallaria*, a representative MSSF, under different flow conditions. We compare our model predictions with the experimental findings, and we use the model to determine whether recirculation is present and how clearance rate changes with organism orientation and strength of the ambient flow.

2. Materials and methods

2.1. Flow measurement

We recorded videos of individual MSSFs attached to the bottom of a rectangular channel with flow driven by a syringe pump (New Era NE-1000) and designed to mimic natural environments (figure 2). The flow in the bottom middle of the channel can be approximated as simple shear flow, $\mathbf{u} = (kz, 0, 0)$, where k is the shear rate and z is the distance above the bottom surface [35]. We performed experiments at a range of flow rates (0.2–10 ml min^{-1}), yielding shear rates of 0.03–3 s^{-1} and channel Reynolds number of $\mathrm{Re} = QD/(Av) = 5$–200. Here, Q is the volume flow rate, v is the kinematic viscosity, and D and A are the depth and cross-sectional area of the channel, respectively. Whether the surface is the floor of a channel, a sphere or the substratum exposed to flow where MSSFs live, simple shear flow is a reasonable first approximation [26].

To make a quantitative connection between shear rates in our experiments and ambient environmental flows, we consider two cases: (i) Blasius boundary layer flow, which is appropriate for flow near a thin flat surface in laminar flow, e.g. a leaf in a pond [26,36], and (ii) turbulent flow near flat surfaces, e.g. a stream bed. Shears of the order of 0.03 s^{-1}, our lowest measured shear rate, would correspond to Blasius flow with free-stream velocity of 700 µm s^{-1} for an MSSF 5 cm from the leading edge. In turbulent flow above a flat smooth surface, this shear rate would correspond to a stream with depth 0.1 m and depth-averaged flow speed of 2 mm s^{-1}. Similarly, our highest measured shear rate of 3 s^{-1} would correspond to Blasius flow with free-stream velocity of about 1 cm s^{-1} for an MSSF 5 cm from the leading edge or turbulent flow for a stream with depth 0.1 m and depth-averaged flow speed of 7 cm s^{-1}. These flow speeds are determined from table 6.1 in [36] and eqns 10 and 13 in [26].

Vorticella convallaria (figure 1*a*) were cultured as in Vacchiano *et al.* [37]. Plastic coverslips (11 mm × 11 mm × 0.1 mm) were left in the cultures overnight, and coverslips with a single *V. convallaria* isolated from neighbours and attached to the thin edge of the coverslip were selected. The coverslip was then inserted into a thin slit in the middle of the channel, such that the edge of the slip with the attached individual was flush with the bottom of the channel (±10 µm). The slit was surrounded by a waterproof chamber to prevent leaks.

High-speed video was recorded for micro-scale particle image velocimetry (µPIV) at 1280 × 800 pixels and a frame rate of 25 or 50 fps using a Phantom v210 camera. The water was seeded with 10 µm neutral-density hollow glass beads (Dantec Dynamics HGS-10). We selected *Vorticella* at a variety of orientations relative to the surface of attachment and all oriented in the plane of view, so that out-of-plane flow was minimized (figure 2 and electronic supplementary material, Movie S1). The channel was illuminated from behind with infrared light, and we estimated the depth of field to be 200 µm. Images were processed in Matlab using custom-written software to select in-focus particles using a threshold in the gradient of the image brightness.

Flow fields were determined using DaVis PIV software (LaVision GmbH, Göttingen, Germany). The organism and surface of attachment were masked manually. We used a multi-pass PIV algorithm with decreasing size of the interrogation windows from 128 × 128 pixels to a final window size of 64 × 64 pixels with 75% overlap. Flow fields were then time averaged over the length of the video.

2.2. Measurement of *Vorticella* orientation

We measured cell body orientation in still water and at shear rates of 0.3 s^{-1}, 0.6 s^{-1} and 1 s^{-1}. Individual *V. convallaria* were imaged in channel flow in a device similar to that described in §2.1, although the channel was 10 mm wide, 8 mm tall and 4 cm long, and individuals were attached directly to the bottom of the channel. Videos were recorded with an Allied Vision Mako camera with a field of view of 1.28 mm × 1.02 mm. Individuals were observed for 6–60 min at 1 fps. In each frame, orientation was determined using a custom-written image-processing routine that fitted the cell body to an ellipse.

Table 1. Examples of flow speeds and types in aquatic environments.

environment	flow type	flow location	flow speed	source
vegetation in shallow stream	unidirectional	5–20 cm above substratum	4 cm s^{-1}	[24]
estuarine mudflats	unidirectional	free stream	6 cm s^{-1}	[25]
rivers and streams	unidirectional	free stream	1–100 cm s^{-1}	[26]
fouling community on a dock	oscillatory	free stream	3–20 cm s^{-1}	[27]
wave-swept rocky shore	oscillatory	free stream	20 cm s^{-1}	[25]
coral reef	oscillatory	free stream	10 cm s^{-1}	[28]
settling marine snow aggregates	unidirectional	sinking speed of aggregate	1 mm s^{-1}	[29]

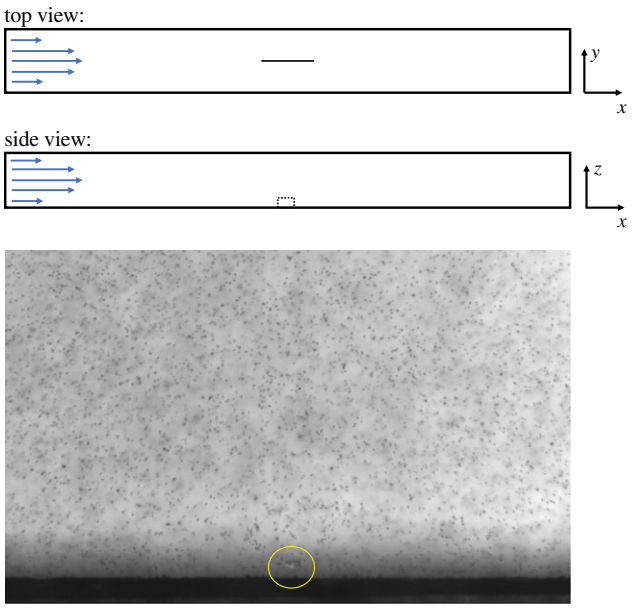

Figure 2. A schematic showing top and side views of a segment of our flow channel. The channel is 8 mm wide, 7 mm tall and 13 cm long. Flow is from left to right (blue arrows). The thin line in the top view indicates the edge of the coverslip inserted into a slit in the bottom of the channel, and the box in the side view indicates the video field of view (2.1 mm × 1.3 mm). The image shows a frame from a typical video with an individual *V. convallaria* circled in yellow (corresponds to electronic supplementary material, Movie S1 and figure 4*c*).

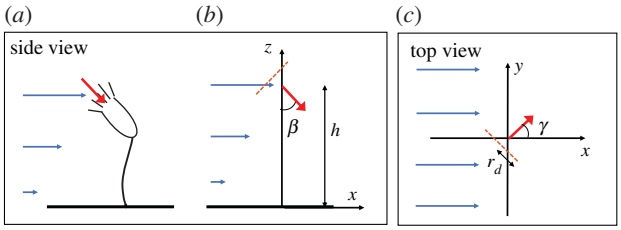

Figure 3. Point-force model in ambient flow. (*a*) Sketch of *Vorticella* with point force (red arrow) and shear flow (blue arrows). (*b*,*c*) Our model with a force at the origin of the red arrow at a distance h above the bottom (thick line). The arrow points in the direction of the force with angles β and γ. The circular feeding disc with radius r_d is indicated by an orange dashed line.

Ellipse orientation and major axis length were used to determine the cell body orientation angle β (figure 3), so β was determined only in the plane of view and not including any tilt towards or away from the camera.

We considered the time-averaged angle of each individual at each shear rate as a measure of typical orientation. To account for individual variation, the deviation in typical angle, $\Delta\beta$, was determined from a reference shear rate (0.6 s^{-1}) for each individual at each flow speed. We assessed statistical significance among time-averaged angles by first performing an ANOVA on a linear mixed effects model to assess if the shear rates affected angle after accounting for individual variation. Then, we performed a *post hoc* least-squares means test to parse out the pairwise differences between each flow rate.

Vorticella orientation was observed to change periodically in time. The peak of the power spectrum of β as a function of time was used to determine the reorientation period. The power spectrum was determined for each individual at each flow speed by performing a fast Fourier transform (FFT) on β as a function of time. Before applying the FFT, the data were high-pass filtered to remove the average angle, low-pass filtered to remove frequencies higher than the Nyquist frequency and windowed using a Blackman–Harris function.

2.3. Model and fitting methods

2.3.1. Point-force model with shear flow

We modelled the MSSF as a point force (stokeslet) above a plane boundary [6,11,20,22,38–40]. This model has been shown to match experiments well for MSSF feeding currents in perpendicular orientations above a single surface and also when confined between two closely spaced surfaces [20–22,41]. We chose this simple low-Reynolds-number model as the *Vorticella* feeding flow has a Reynolds number of approximately 10^{-3} [6], and because we hope to find the simplest model that accurately predicts zones of recirculation and allows us to determine how clearance rates vary with feeding angle and ambient flow speed.

The point force is located at height h above the surface and pushes the fluid with force f. Its orientation relative to the surface is described by angles β and γ (figure 3). To complete this model, we represented the ambient flow as simple shear flow: $\mathbf{u} = (kz, 0, 0)$ as discussed above (§2.1).

To describe the flow topology and determine which parameter combinations lead to recirculation, we numerically determined the location of critical points and classified them using the eigenvalues of the Jacobian matrix [42]. Critical points that are centres, attracting foci or repelling foci can indicate zones of recirculation, which we define as closed streamlines or spirals. Other critical points (e.g. saddle points) do not indicate zones of

recirculation. We examined the case where $\gamma = 0$ and determined critical points in the symmetry plane ($y = 0$).

2.3.2. Scaling

We use dimensionless variables indicated by an asterisk. Lengths are scaled by h. Velocities, times, shear rates and clearance rates are scaled by their characteristic scales

$$v_0 = \frac{f}{\mu h}, \quad t_0 = \frac{\mu h^2}{f}, \quad k_0 = \frac{f}{\mu h^2} \quad \text{and} \quad Q_0 = \frac{fh}{\mu},$$

where μ is the viscosity. We observe average values of $h = 190 \pm 20$ µm and $f = 230 \pm 30$ pN, where ± indicates standard error. Using these average values and the viscosity of water gives $v_0 \approx 1000$ µm s^{-1}, $t_0 \approx 0.2$ s, $k_0 \approx 6$ s^{-1} and $Q_0 \approx 4 \times 10^{-11}$ m^3 s^{-1}.

2.3.3. Fitting to experiment

We fitted the calculated flow fields to the experimental flow fields using least-squares regression. The fitting of the background flow and that of the point-force flow were conducted separately. The background velocity was fitted to $v_b(z) = k(z - z_s)$, where the two fitted parameters were the shear rate, k, and the position of the surface, z_s. We took the average of the fits to the left and right of the cell. Any measurements for which the fits between the linear speed profile and the experimental flow field had an error greater than 10% were removed.

We then subtracted the fitted background flow so the resulting flow was a *Vorticella* in isolation. We next fitted the point-force flow to the experimental flow, where the fitting parameters were the x and z location, the direction and the magnitude of the force. We confined the fitted x and z coordinates to within a cone based on the measured position of the *Vorticella*. The cone had an opening angle of 40° and radius of 1.05h, and the tip of the cone was 0.05h below the measured cell body position tilted by the measured cell body angle. The point-force fitting was confined to the flow-field data within an annulus centred on the cell (inner radius of 250 µm and an outer radius of 500 µm). As with the fits to the background flow, any fit between point-force flow and experimental flow where the error was greater than 10% was removed. Four flow fields were removed for this reason; all were at our highest flow velocities (0.8–2.8 s^{-1}), where the feeding flow is a small fraction of the total flow and the determination, by subtraction, of the *Vorticella* flow field becomes uncertain. Thus, the failure of these fits reveals the upper limit on flow velocity for our fitting procedure.

2.3.4. Clearance rates

We calculated clearance rates as a function of time from the combined point-force and simple-shear flow as the fluid flux across a feeding disc located in a plane perpendicular to the point force and centred on a line passing through it (figure 3*b*,*c*) [6]. A grid of fluid particles located on the feeding disc was followed backwards in time according to the velocity field. Initially, each grid element of the feeding disc contributed $\mathbf{u} \cdot d\mathbf{A}$ to the clearance rate, where $\mathbf{u}$ is the fluid velocity at the centre of the grid element and $d\mathbf{A}$ is a vector whose magnitude is the area of the grid element and whose direction is perpendicular to the feeding disc. If a fluid particle recirculated and returned to the feeding disc, then that element of the grid no longer contributed to the clearance rate. An alternative approach would be to find the clearance rate by using simulations to fully solve the advection–diffusion equation (e.g. [6,43]).

We determined the size of the feeding disc experimentally by imaging feeding *Vorticella* and tracing captured particles backwards in time (electronic supplementary material, SI §1). Using this measured capture zone, along with the average point-force height, $h = 190$ µm, we find a disc radius, $r_d/h = 0.1$, which we used in all clearance rate calculations. We also set the feeding disc a distance of 0.1h in front of the point force to avoid including the singularity within the feeding disc.

3. Results

3.1. Measured flow fields

When *Vorticella* are exposed to ambient flow, recirculation in the feeding current is reduced or eliminated for organisms that are perpendicular to the surface (figure 4*a*) or lean upstream (figure 4*b*), but not for those that lean downstream (figure 4*c*). We measured flow for *Vorticella* angles ranging from $\beta = 70° \pm 15°$ to $\beta = -110° \pm 15°$ at shear rates from 0 s^{-1} to 2.8 s^{-1}. Details of all measured flows are in electronic supplementary material, SI §2 and flow fields are available in the Dryad data repository [44]. We observed no recirculation in the feeding current at any ambient flow condition for $\beta \geq 0°$, i.e. those that lean upstream and, thus, have a component of their feeding current in the same direction as the ambient flow. For negative angles, recirculation was more likely to be present if ambient flow was slow and if the feeding current was directed opposite the ambient flow.

3.2. Measured *Vorticella* orientations

As in still water [6], we observe that *Vorticella* in flow typically have a periodic pattern of active reorientation in time with a period of about 200 s (figure 5*a*,*b*). Within this periodic variation the typical orientation angle for β varies among individuals (figure 5*c*). There is also variation among individuals in the breadth of angles explored (figure 5*c*). However, there is a clear pattern that at higher shear rates the organisms are more likely to be tilted downstream and pulling fluid opposite the direction of ambient flow (figure 5*d*).

3.3. Model results

3.3.1. Model validation

Calculated flow fields matched experimental flow fields well (figure 4 and table 2). For the 17 flow fields that we were able to fit to calculations, there was a qualitative match between experiment and calculation for the presence or absence of recirculation, and the general location and size of the region of recirculation (see electronic supplementary material, SI §2 for details of these fields and the Dryad data repository for model results for all flow fields [44]). There was also a qualitative match between experiment and calculation for the presence or absence of recirculation for the five flow fields that we could not fit to our model, and which we compared with calculations with average *Vorticella* parameters (electronic supplementary material, SI §2). This robust match between experiment and calculation means that our model is sufficient to predict the structure of recirculation in the flow, and therefore to predict, at least qualitatively, how clearance rates vary with time and organism orientation.

To determine the extent to which our model can be used to make quantitative predictions, we compared the clearance rates across the feeding disc predicted by our calculations with those measured using PIV (electronic supplementary material, SI §3). Across the flow speeds and orientations that we measured, these results showed a good match in

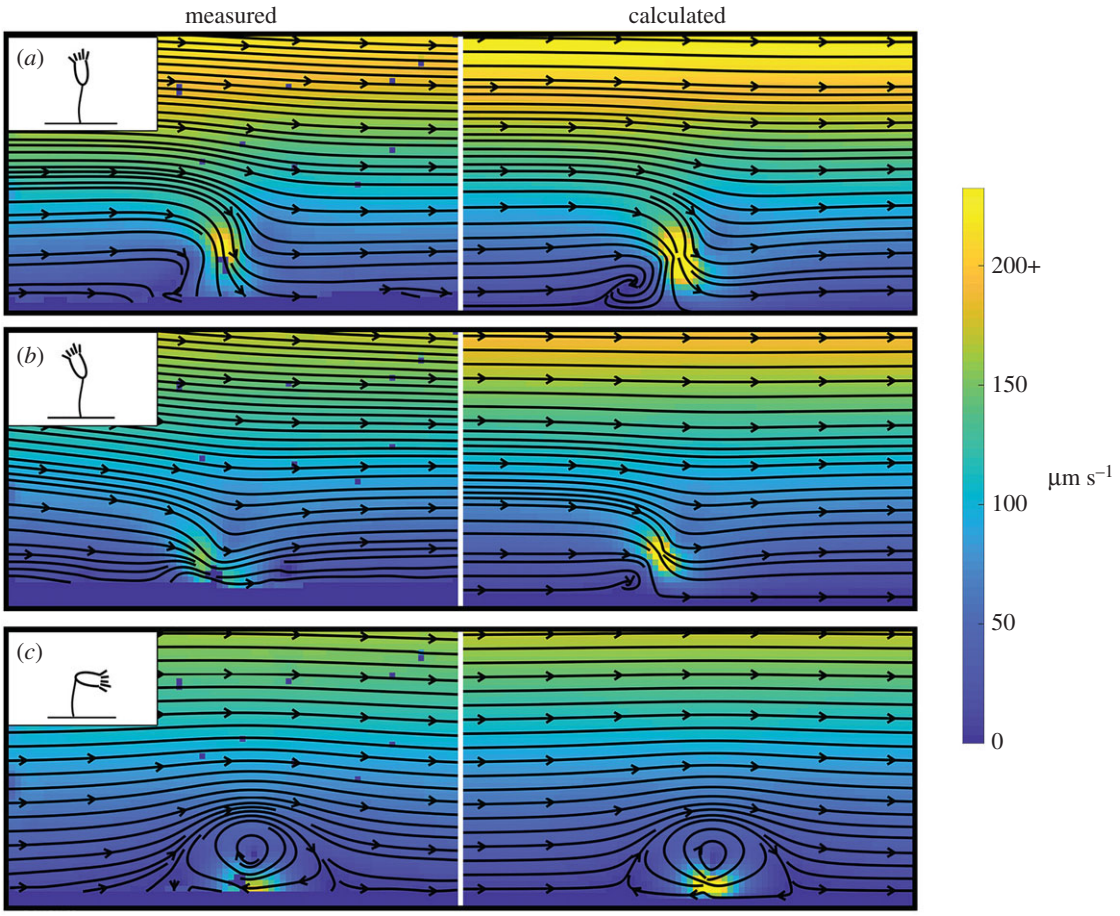

Figure 4. The flow fields of *Vorticella* in ambient flow at different orientations. (*a*) *Vorticella* approximately perpendicular, (*b*) tilted upstream and (*c*) tilted downstream. Black lines are approximate streamlines and colours indicate speed. The field of view is 2.1 × 1.3 mm. The *Vorticella* is located in the bottom middle, at the area of high flow magnitude, and has orientation as shown in the upper-left inset. In each box, the left panel is the measured flow and the right panel the model flow. Note that the colour scale is capped at the maximum experimental value in (*a*), and that $\gamma = 0$ for all calculated fields. Model parameters are shown in table 2.

Table 2. Fitted model parameters for flow fields in figure 4.

figure 4 panel	β (°)	h (μm)	f (pN)	k (s^{-1})	k^*
a	8	270	370	0.18	0.04
b	26	200	200	0.16	0.03
c	−110	70	290	0.14	0.002

trend, although not an exact match in values: clearance rates matched within an order of magnitude, and calculated clearance rates always overestimate measured rates, typically by a factor of 3–4.

Our clearance rates also match well previously measured clearance rates. Sanders *et al.* used uptake of fluorescent beads and bacteria and found clearance rates for *V. convallaria* of $1 \times 10^5 - 5 \times 10^5$ μm^3 s^{-1} [45], comparable to the median value of 2×10^5 μm^3 s^{-1} for our experimental data (see electronic supplementary material, SI figure S2 for the full range). Similar measurements of clearance rates based on bead uptake for other *Vorticella* species found clearance rates from 5×10^4 μm^3 s^{-1} to 2×10^7 μm^3 s^{-1}, and a determination of clearance rate from the measured flow field of *Vorticella picta* is also within that range [2,46,47].

There are two areas where the model and experiment do not agree: (i) near the point force, where its singular nature leads to unrealistically large velocity magnitudes; and (ii) at the cell body, where the μPIV is less accurate than in other regions and the point-force model ignores flow disturbance due to the cell body. While details of the flow in these regions are not needed for our analysis of clearance rate, our model could be modified to use a regularized stokeslet to better match these near-field flows [48].

Overall, our model captures well the structure of the flow field and accurately determines in what situations recirculation will reduce clearance rates. Quantitative values for clearance rates from our calculations are overestimates that are correct within an order of magnitude.

3.3.2. Flow topology

Our model shows a variety of flow structures (figure 6). We find smooth streamlines and no recirculation when $\beta = 90°$ (figure 6*a*). Areas of recirculation appear and become larger as β approaches −90° (figure 6*b–d*). Increasing flow speed causes the zone of recirculation to become smaller (figure 6*d* versus figure 6*f*). We can calculate analytically the location of the stagnation points at the centres of the eddies for the special case of $\beta = -90°$, where there is symmetry across the point force in the x-direction. We found that there are always two stagnation points, with the lower one very near the bottom surface at slower flows (figure 6*h*). As flow speed increases, the two stagnation points move closer to the stokeslet, leading to a smaller zone of recirculation with two defined eddies (figure 6*f*,*h*). In general,

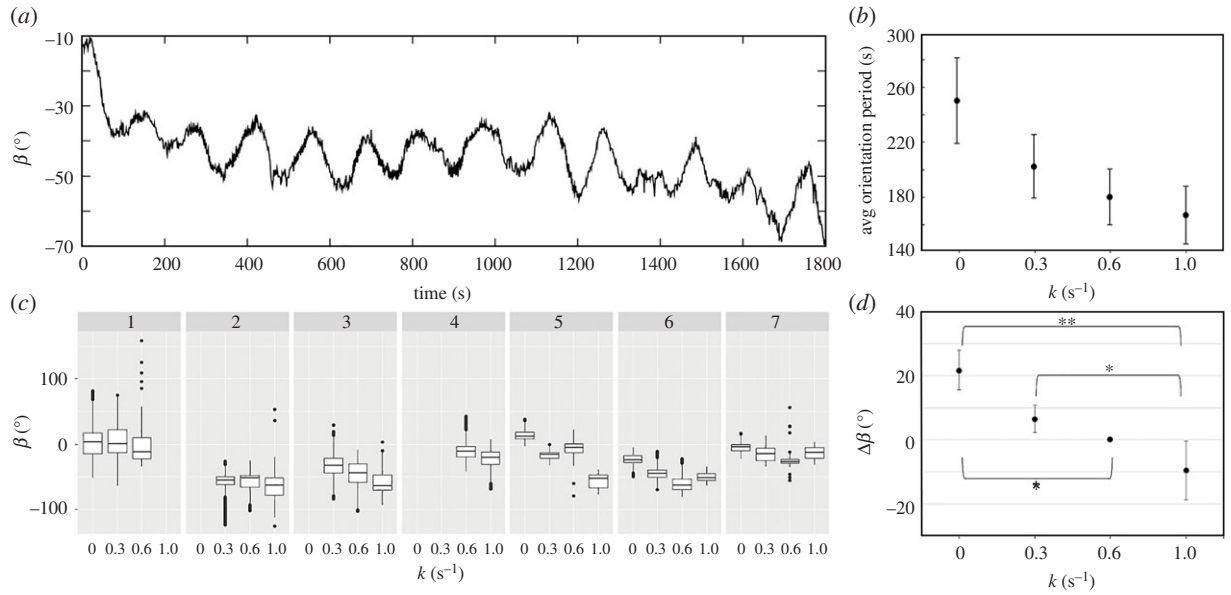

Figure 5. (*a*) Example of the pattern of orientation angle in time for *Vorticella* in flow (individual 6 at $k = 0.3\ s^{-1}$ in (*c*)). (*b*) Reorientation period as a function of shear rate. $N = 3$ for still water, $N = 4$ for $k = 0.6\ s^{-1}$ and $N = 6$ for other orientations; error bars are standard error of the mean. The trend is not significant; $p = 0.06$ for a generalized linear model with a gamma distribution. (*c*) Orientation angle, β, as a function of shear rate, k, for seven different *Vorticella* (individual indicated by numbers in grey bars at top). The box shows the lower and upper quartiles of angles explored by the organisms. The horizontal bar indicates the median angle, the error bars are 1.5 × the quartile boundaries and dots show any instances of angles measured beyond the bounds of the error bars. (*d*) Change in typical orientation angle, $\Delta\beta$ (see §2.2 for definition), as a function of shear rate ($N = 4$ for still water, $N = 7$ for $k = 0.6\ s^{-1}$ and $N = 6$ for other orientations). Error bars are standard error of the mean. Asterisks indicate statistically significant differences (*post hoc* least-squares means test): * indicates $p \leq 0.05$ level and ** indicates $p \leq 0.01$ level.

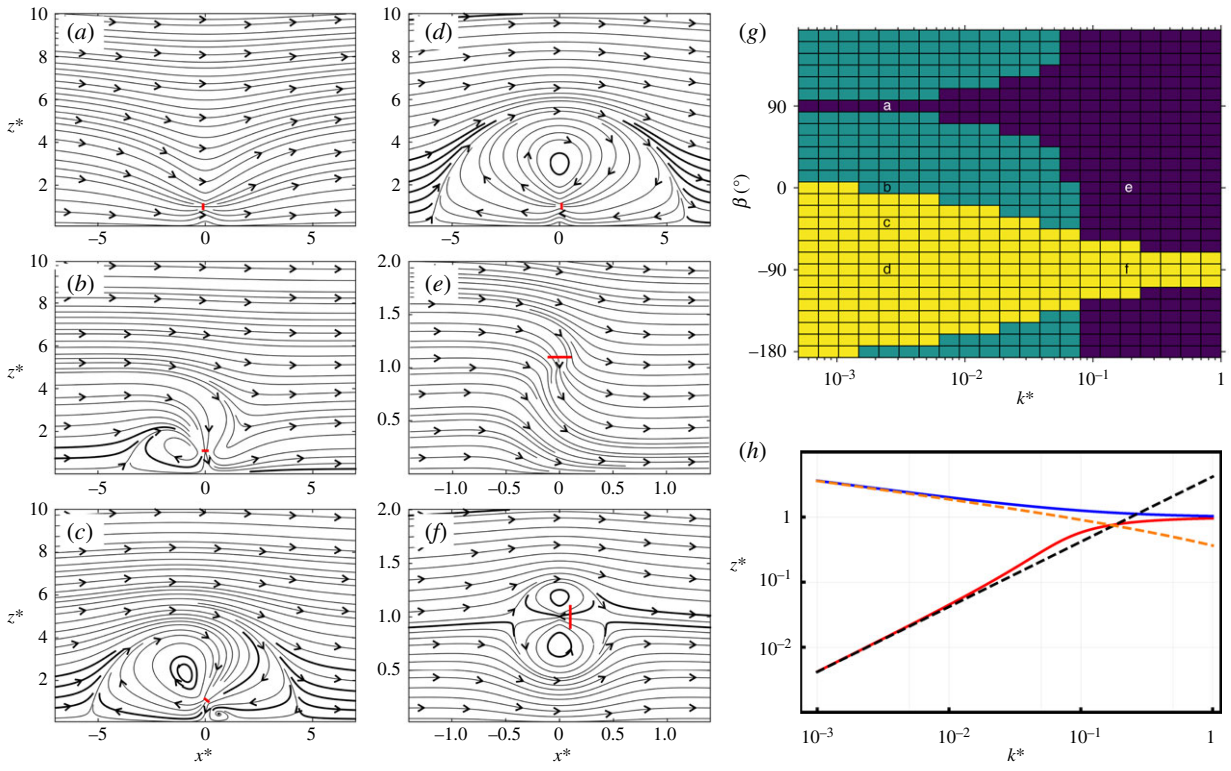

Figure 6. (*a–f*) Approximate streamlines from our model; the point force is at (0,1) and the bottom surface at $z = 0$. The red line indicates a feeding disc with $r_d/h = 0.1$. For (*a–d*) $k^* = 2 \times 10^{-3}$; for (*e*) and (*f*) $k^* = 2 \times 10^{-1}$. (*g*) Classification of flow structures in the symmetry plane for $\gamma = 0$. Yellow indicates two areas of recirculation; turquoise indicates one area of recirculation; dark blue indicates no recirculation. Letters correspond to parameters used in streamline plots. (*h*) The height of the stagnation points at the centre of the two eddies for $\beta = -90°$. The solid lines represent exact locations, while the dashed lines represent approximations for $k^* \ll 1$: $z^*_{\text{lower}} \approx 4\pi k^*/3$ and $z^*_{\text{upper}} \approx (4\pi k^*/3)^{-1/4} - 1/3$.

we found that, as ambient flow speed increases, fewer angles lead to recirculation (figure 6*g* and figure 6*b* versus figure 6*e*). These model results match our experimental observations (figure 4). Furthermore, while closed streamlines in the symmetry plane occur at many angles, we only see closed streamlines elsewhere for $\beta = -90°$. Clearance rates will be reduced by recirculation only if the feeding disc intersects recirculating streamlines (e.g. figure 6*d*,*f*).

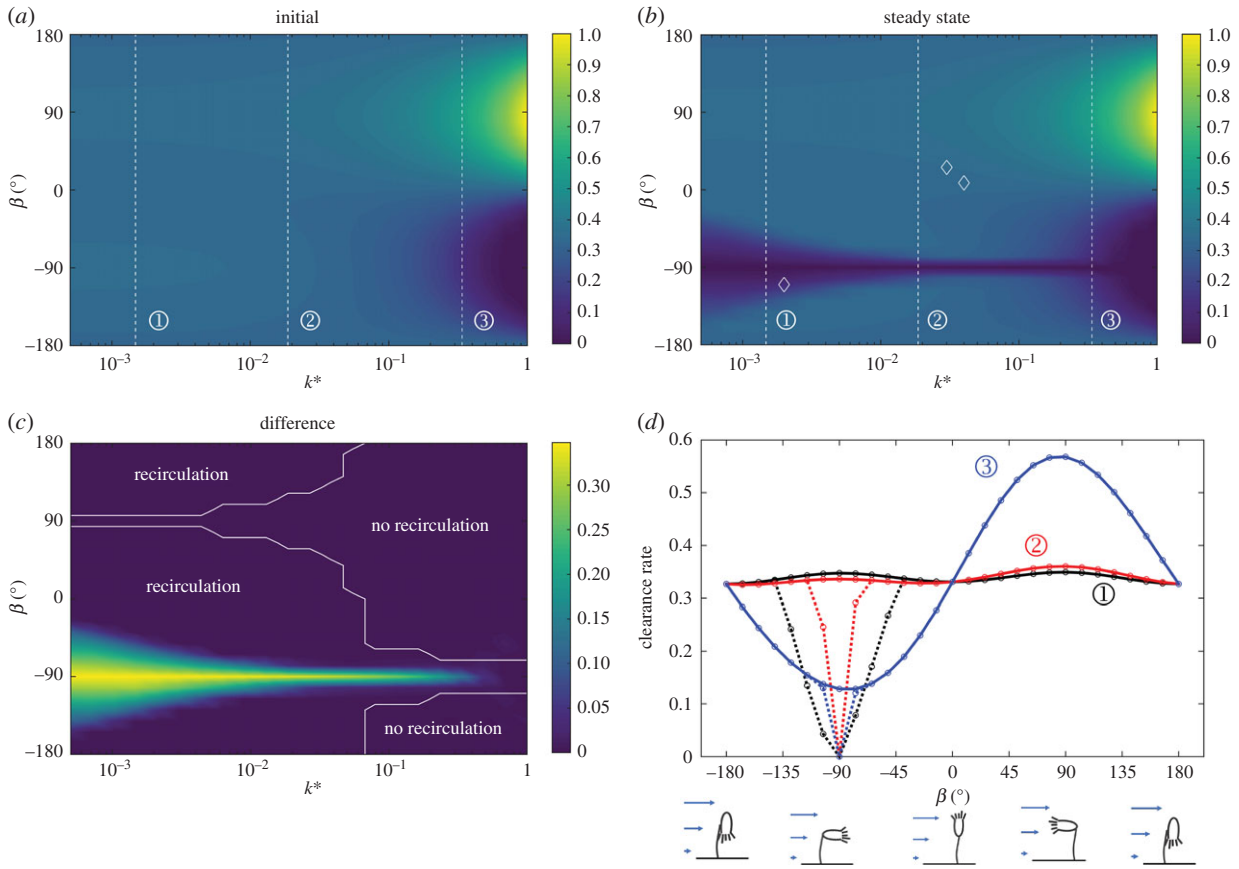

Figure 7. Normalized clearance rates for model *Vorticella*. Clearance rates in all panels are normalized by the maximum clearance rate in (*a*) of 0.048. In dimensional units 0.048 corresponds to a clearance rate of 2×10^{-12} m^3 s^{-1}. (*a*) Initial clearance rates (i.e. at time = 0 and no recirculation yet), indicated by colour, as a function of feeding angle and shear rate. Dashed lines correspond to data used in (*d*). (*b*) Steady-state clearance rates (i.e. all recirculating streamlines have recirculated) indicated by colour, as a function of feeding angle and shear rate k^*. Dashed lines correspond to data in the plots in (*d*). Diamonds show the parameters for the flow fields in figure 4 and table 2. (*c*) Normalized difference between initial and steady-state clearance rates. Larger values indicate a greater reduction in clearance rate due to recirculation. White lines indicate whether recirculation is present in the flow (based on figure 6). (*d*) Normalized clearance rate as a function of feeding angle for the dashed-line transects in (*a*) and (*b*): $k^* = 3.3 \times 10^{-1}$ (blue line), $k^* = 1.8 \times 10^{-2}$ (red line) and $k^* = 1.5 \times 10^{-3}$ (black line). Solid lines indicate initial clearance rates, while dashed lines indicate steady-state clearance rates. Representative *Vorticella* body positions are shown for several values of β.

3.3.3. Clearance rates for perpendicular orientation

Even very slow ambient flow can change the recirculation around perpendicular MSSFs such that the feeding disc no longer intersects recirculating streamlines. With our choice of feeding disc, we find that a shear rate of $k^* = 2 \times 10^{-6}$ is the minimum shear rate needed to ensure a constant supply of fresh food to the entire feeding disc for a perpendicular cell. For our scaling (§2.3.2), this is a shear rate of 10^{-5} s^{-1}, corresponding to a free-stream velocity of about 4 µm s^{-1} in laminar Blasius flow or a turbulent stream with depth-averaged flow speed of 8 µm s^{-1}, calculated using the same assumptions as in §2.1. These shear rates are orders of magnitude smaller than those that produce flow of similar speed to the *Vorticella* feeding current ($k^* \sim 1$). This is because, for perpendicular feeders in still water, the region of recirculating eddies that intersect the feeding disc extend tens of body lengths into the water column and recirculate very slowly [6,23]. They are, thus, easily disrupted by flow. Similarly, larger feeding discs would require faster flow to disrupt all recirculating streamlines that intersect the feeding disc, as larger discs include streamlines further from the point force that extend less far into the water column and recirculate more quickly.

3.3.4. Clearance rates for other orientations

We first consider orientations with no cross-flow component ($\gamma = 0$; figure 7). The best orientation for feeding is tilted directly upstream into the flow ($\beta = 90°$), with feeding current and ambient flow working together. The lowest clearance rates happen at the opposite orientation, when the organism is tilted directly downstream with the feeding current in the opposite direction to the ambient flow ($\beta = -90°$).

Even when the feeding current speed is greater than the ambient flow speed, clearance rates for organisms tilted downstream and pushing against the ambient flow reduce to zero or near zero in time (figure 7*b*,*d*). This occurs because the entire feeding disc is within an area of recirculation. For slower flow (smaller k^*), a larger range of β angles centred on –90° have clearance rates reduced by recirculation (figure 7*c*,*d*). Slow ambient flow does not directly affect the initial clearance rate through the feeding disc significantly when $k^* < 10^{-1}$ (figure 7*a*), but it influences the steady-state clearance rate by changing the overall flow structure and recirculation pattern (figure 7*b*), since the flow speeds in the self-generated feeding current are very low in the far field where the closed streamlines return [23,39].

These results are opposite those in still water (figure 1), where the perpendicular orientation has a reduced clearance rate due to recirculation, and the parallel orientation is free from recirculation [6,19].

We also find that larger feeding discs relative to stalk length experience reduced clearance rates at a larger range of angles and flow speeds than smaller ones, and the time to first recirculation decreases with increasing disc size

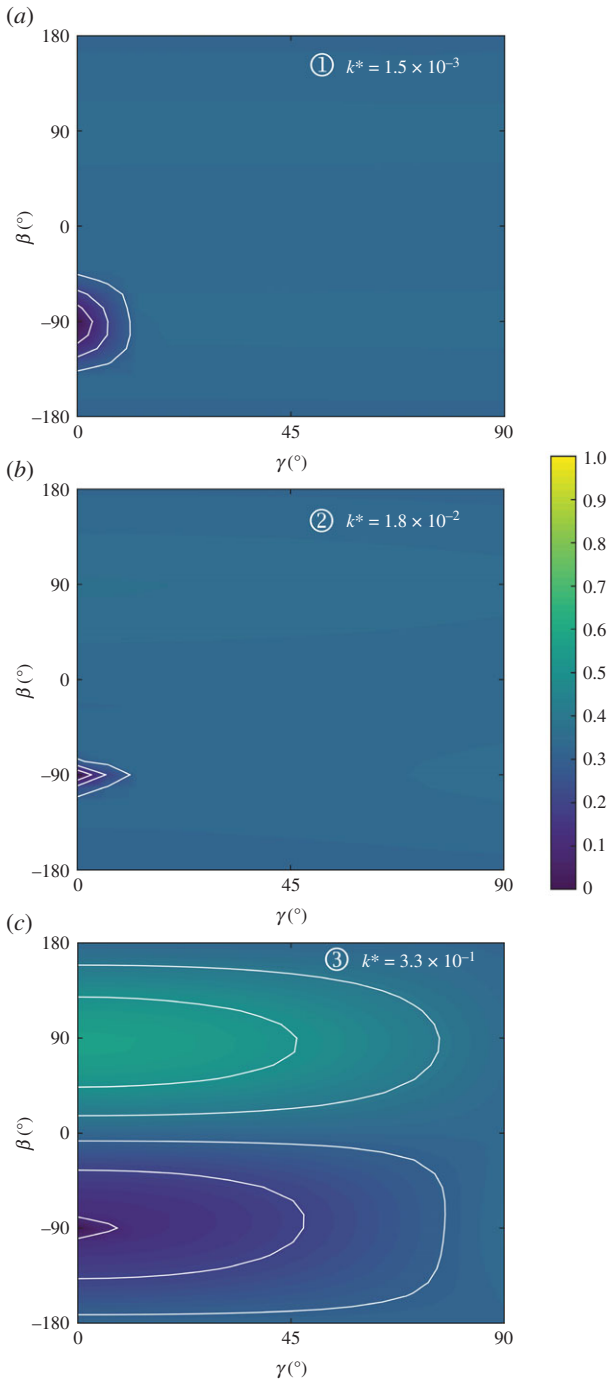

Figure 8. Steady-state clearance rate, indicated by colour, as a function of β and γ. The clearance rate is normalized by the maximum rate in figure 7*a* of 0.048, and contour lines are at intervals of 0.1. The shear rates correspond to dashed lines in figure 7*a*,*b*.

(electronic supplementary material, SI §6). However, clearance rates are overall larger for larger discs, since there is more area encountering fluid.

If the organism tilts in the cross-flow direction (non-zero γ), the extent of recirculation in the flow is reduced (figure 8). Only orientations that have a significant component of feeding force pointing against the flow, and minimal component in the cross-flow direction, result in reduced steady-state clearance rates.

Overall, there are distinct angles at which clearance rate reduces to zero with time for MSSFs in shear flow. These angles centre on $\beta = -90°$ and $\gamma = 0°$, and the range of affected angles is larger for organisms in slower flow or with larger feeding discs relative to stalk lengths.

4. Discussion

We found that clearance rates for MSSFs depend on both organism orientation and ambient flow conditions. Therefore, to predict and understand clearance rates in nature, one must understand both typical ambient flows and typical organism orientations. Clearance rates of protists have often been determined by measuring the rate at which inert particles or fluorescently labelled prey are consumed (e.g. [10,33,49]). However, these types of measurements give clearance rates that vary widely, even among individuals of the same species [50]. This could simply be due to different ambient flow conditions and cell orientations among individuals.

We also found that perpendicular MSSFs have a constant supply of food for nearly all natural environments, as they do not experience recirculation through the feeding disc even for ambient flows much slower than found in most natural environments (table 1). We therefore expect that organisms in natural habitats will not experience the feeding restrictions due to eddies described in previous work on MSSFs at perpendicular orientations in still water [6,18,20,21,40].

At all ambient flow speeds we studied, individual *Vorticella* explored a range of orientations, demonstrating that they maintain the ability to actively reorient (§3.2). However, as the ambient flow speed increased, the active reorientation patterns became biased towards downstream tilt, leading to decreased initial clearance rates. It is possible that this decrease could be mitigated by some cross-flow tilt. We also rarely observed organisms oriented directly upstream at the angle that maximizes clearance rate, though, from our sample, it is difficult to determine if this is due to the ambient flow. At higher ambient flow speeds, drag forces on the cell body may become strong enough to overpower active motion of the *Vorticella* and force it to align with the flow. This could force organisms into the 'danger zone' where recirculation would eventually cause clearance rates to decrease to zero. In our model (which mimics *Vorticella*), tilted downstream means $\beta \approx -90°$ and low clearance rates. However, choanoflagellates push fluid in the opposite direction. Thus, forces from ambient flow would assist choanoflagellates anchoring in a favourable orientation, but hinder *Vorticella*. These results also highlight that MSSFs that anchor solidly with a set orientation relative to the surface may be able to feed more effectively in regions with fast flow than MSSFs with a flexible stalk.

In slow flows, *V. convallaria* reorient quickly enough to escape any decrease in clearance rates due to recirculation. To determine this for *Vorticella*, and similar species that actively control their orientation, we can compare the time scale of organism reorientation with the time scale of the recirculating flow. For *V. convallaria*, we found that the time at which recirculation first occurs (the time for depleted fluid to first return to the feeding disc) scaled approximately inversely with shear rate (electronic supplementary material, SI §4). The range of non-dimensional recirculation times predicted corresponds to 10^{-3} s to 30 min. It has previously been shown that *V. convallaria* reorient themselves with a time scale of minutes [6], and we found in our experiments that this general time scale is robust across individuals and flow speeds (§3.2). Here, flow where *Vorticella* would reorient quickly enough to avoid recirculation corresponds to Blasius flow with a free-stream velocity of 3 mm s^{-1} or a turbulent stream with a depth-averaged flow speed of 6 mm s^{-1}, using the same assumptions as in §2.1. Frequent reorientation

of the cell body would also limit the impact of recirculation at higher velocities, as the decreased clearance rate would only last for times on the scale of minutes before reorientation would bring in fresh fluid. We suggest that the ability to reorient actively is an advantage to benthic MSSFs as it may limit the effect of recirculation on clearance rate.

Our results also demonstrate the benefits of a longer stalk. One aspect of this benefit has long been known: moving away from the surface leads to higher feeding flow speeds and, thus, larger clearance rates [11,23]. Our results revealed that organisms with a short stalk for a given feeding disc size experienced a clearance rate reduction for a larger range of angles than those with a long stalk (electronic supplementary material, SI §6). Thus, having a longer stalk also helps an organism avoid regions of recirculation in the flow.

Clearance rate is also affected by the force an organism can apply to the fluid, which varies both among individuals of the same species and among different species. Without external flow, clearance rate is proportional to this force. In flow, a stronger force reduces the effect of ambient flow, i.e. reduces k^* for a given flow speed, and, therefore, leads to recirculation at a wider range of angles. We found a range of forces from 100 to 500 pN for *V. convallaria*, which matches well ranges reported for similar organisms [6,21].

While our results do not include the diffusion or swimming of food particles, it would be interesting to investigate further, as diffusive motion of prey has been shown to reduce the effect of recirculation in still water for prey that diffuse quickly [6]. Scaling estimates of the Péclet number for our flow fields (electronic supplementary material, SI §5) indicate that flow dominates over diffusion in most situations, but diffusion may become important for *Vorticella* feeding on fast motile bacteria in slow ambient flow or for the very small eddies seen in faster ambient flow.

5. Conclusion

Both initial and steady-state clearance rates for MSSFs depend strongly on the interaction between the ambient flow and the organism orientation and body plan (e.g. stalk length, feeding disc size and direction of feeding force). Even flow much slower than that found in nearly all natural environments is enough to disrupt the recirculation around perpendicular MSSFs. However, ambient flow typical of natural habitats can help or hinder organism feeding. This depends on the ability of the organism to adjust its orientation and whether it pushes the water away from or towards the surface of attachment.

Furthermore, many MSSFs have the ability to detach and relocate and therefore to find attachment positions that are optimal for feeding under the prevailing flow conditions. The flow conditions for surfaces of attachment in the environment vary substantially. Waving leaves and sinking marine snow aggregates are moderate- to high-flow environments, while sediments are low-flow environments. In addition, there will be steep micro-scale spatial gradients in flow conditions in these complex three-dimensional environments. One could therefore expect that organisms with different body plans adapted to different environments would demonstrate similar macro- and micro-scale distributional patterns. Although much is known about the ecological distributions and roles of MSSFs (e.g. [4,9,10,12]), the patterns of distribution of different morphotypes in measured flow microhabitats in the field have not been studied.

The feeding currents of MSSFs not only provide the individual organism with food but may also affect large-scale mass transport by eroding or thinning viscous boundary layers. Thus, MSSFs attached to a seagrass leaf may enhance the transport of oxygen and carbon dioxide between the leaves and the environment, and MSSFs attached to marine snow particles or sewage flocs may similarly affect encounter rates, coagulation rates and solute transport. With an understanding of the adaptive values of different types of feeding flows and body plans, the potentially important larger-scale implications of MSSFs on system processes can now be explored, whether it is productivity of seagrasses or particle coagulation. Our results show that, in order to understand these larger-scale ecological roles played by MSSF pumping and feeding, we must study these functions under realistic ambient water flow conditions.

Data accessibility. Original PIV flow-field data for all measured flow fields are available in the Dryad data repository [44].

Authors' contributions. R.E.P., M.A.R.K., T.K. and A.A. designed the research; R.E.P., T.H. and L.T.N. carried out the experiments; R.E.P., E.E.R. and M.B. performed model simulations; and R.E.P., E.E.R., T.K. and A.A. wrote the paper with comments from M.B., T.H., L.T.N. and M.A.R.K.

Competing interests. We declare we have no competing interests.

Funding. We are grateful for support from NSF grant no. IOS-1755326 to R.E.P., NSF grant no. IOS-1655318 to M.A.R.K., The Independent Research Fund Denmark (grant no. 7014-00033B) to T.K. and A.A., the European Union's Horizon 2020 research and innovation programme under the Marie Skłodowska-Curie grant agreement no. 713683 to E.E.R., and the Miller Institute for Basic Research in Science (postdoctoral fellowship to R.E.P.). The Centre for Ocean Life is supported by the Villum Foundation.

Acknowledgements. We are thankful for help from Sangjin Ryu, Bob Peaslee, Erik Hansen, Brett Klaassen van Oorschot, Deniz Senyuz, Olivia Perotti, Ulrich Hoff and Kirstine Berg-Sørensen.

References

1. Dopheide A, Lear G, Stott R, Lewis G. 2009 Relative diversity and community structure of ciliates in stream biofilms according to molecular and microscopy methods. *Appl. Environ. Microbiol.* **75**, 5261–5272. (doi:10.1128/AEM.00412-09)
2. Kankaala P, Eloranta P. 1987 Epizooic ciliates (*Vorticella* sp.) compete for food with their host *Daphnia longispina* in a small polyhumic lake. *Oecologia* **73**, 203–206. (doi:10.1007/BF00377508)
3. Sieburth JMcN. 1984 Protozoan bacterivory in pelagic marine waters. In *Heterotrophic activity in the sea* (eds JE Hobbie, PJ Williams), NATO Conference Series, pp. 405–444. New York, NY: Springer.
4. Taylor WD. 1983 A comparative study of the sessile, filter-feeding ciliates of several small streams. *Hydrobiologia* **98**, 125–133. (doi:10.1007/BF02185630)
5. Šimek K, Jezbera J, Horňák K, Vrba J, Sed'a J. 2004 Role of diatom-attached choanoflagellates of the genus *Salpingoeca* as pelagic bacterivores. *Aquatic Microb. Ecol.* **36**, 257–269. (doi:10.3354/ame036257)
6. Pepper RE, Roper M, Ryu S, Matsumoto N, Nagai M, Stone HA. 2013 A new angle on microscopic suspension feeders near boundaries. *Biophys. J.* **105**, 1796–1804. (doi:10.1016/j.bpj.2013.08.029)

7. Azam F, Fenchel T, Field JG, Gray JS, Meyer-Reil LA, Thingstad F. 1983 The ecological role of water-column microbes in the sea. *Mar. Ecol. Prog. Ser.* **10**, 257–263. (doi:10.3354/meps010257)
8. Sherr EB, Sherr BF. 2002 Significance of predation by protists in aquatic microbial food webs. *Antonie Van Leeuwenhoek* **81**, 293–308. (doi:10.1023/A:1020591307260)
9. Finlay BJ, Esteban GF. 1998 Freshwater protozoa: biodiversity and ecological function. *Biodivers. Conserv.* **7**, 1163–1186. (doi:10.1023/A:1008879616066)
10. Fenchel T. 1980 Suspension feeding in ciliated protozoa: feeding rates and their ecological significance. *Microb. Ecol.* **6**, 13–25. (doi:10.1007/BF02020371)
11. Fenchel T. 1986 Protozoan filter feeding. *Prog. Protistol.* **1**, 65–113.
12. Fenchel T. 1987 *Ecology of protozoa: the biology of free-living phagotrophic protists*. New York, NY: Springer-Verlag
13. Eisenmann H, Letsiou I, Feuchtinger A, Beisker W, Mannweiler E, Hutzler P, Arnz P. 2001 Interception of small particles by flocculent structures, sessile ciliates, and the basic layer of a wastewater biofilm. *Appl. Environ. Microbiol.* **67**, 4286–4292. (doi:10.1128/AEM.67.9.4286-4292.2001)
14. Reid R. 1969 Fluctuations in populations of 3 *Vorticella* species from an activated-sludge sewage plant. *J. Eukaryot. Microbiol.* **16**, 103–111. (doi:10.1111/j.1550-7408.1969.tb02240.x)
15. Gertler C, Näther DJ, Gerdts G, Malpass MC, Golyshin PN. 2010 A mesocosm study of the changes in marine flagellate and ciliate communities in a crude oil bioremediation trial. *Microb. Ecol.* **60**, 180–191. (doi:10.1007/s00248-010-9660-3)
16. Fried J, Lemmer H. 2003 On the dynamics and function of ciliates in sequencing batch biofilm reactors. *Water Sci. Technol.* **47**, 189–196. (doi:10.2166/wst.2003.0316)
17. Rehman A, Shakoori FR, Shakoori AR. 2010 Resistance and uptake of heavy metals by *Vorticella microstoma* and its potential use in industrial wastewater treatment. *Environ. Prog. Sustain. Energy* **29**, 481–486. (doi:10.1002/ep.10450)
18. Higdon JJL. 1979 The generation of feeding currents by flagellar motions. *J. Fluid Mech.* **94**, 305–330. (doi:10.1017/S002211207900104X)
19. Liron N, Blake JR. 1981 Existence of viscous eddies near boundaries. *J. Fluid Mech.* **107**, 109–129. (doi:10.1017/S0022112081001699)
20. Blake JR, Otto SR. 1996 Ciliary propulsion, chaotic filtration and a 'blinking' stokeslet. *J. Eng. Math.* **30**, 151–168. (doi:10.1007/BF00118828)
21. Hartmann C, Özmutlu Ö, Petermeier H, Fried J, Delgado A. 2007 Analysis of the flow field induced by the sessile peritrichous ciliate *Opercularia asymmetrica*. *J. Biomech.* **40**, 137–148. (doi:10.1016/j.jbiomech.2005.11.006)
22. Roper M, Dayel MJ, Pepper RE, Koehl MAR. 2013 Cooperatively generated stresslet flows supply fresh fluid to multicellular choanoflagellate colonies. *Phys. Rev. Lett.* **110**, 228104. (doi:10.1103/PhysRevLett.110.228104)
23. Rode M, Meucci G, Seegert K, Kiørboe T, Andersen A. 2020 Effects of surface proximity and force orientation on the feeding flows of microorganisms on solid surfaces. *Phys. Rev. Fluids* **5**, 123104. (doi:10.1103/PhysRevFluids.5.123104)
24. Sand-Jensen K, Mebus JR. 1996 Fine-scale patterns of water velocity within macrophyte patches in streams. *Oikos* **76**, 169–180. (doi:10.2307/3545759)
25. Lau WWY, Martinez MM. 2003 Getting a grip on the intertidal: flow microhabitat and substratum type determine the dislodgement of the crab *Pachygrapsus crassipes* (Randall) on rocky shores and in estuaries. *J. Exp. Mar. Biol. Ecol.* **295**, 1–21. (doi:10.1016/S0022-0981(03)00276-4)
26. Silvester NR, Sleigh MA. 1985 The forces on microorganisms at surfaces in flowing water. *Freshwater Biol.* **15**, 433–448. (doi:10.1111/j.1365-2427.1985.tb00213.x)
27. Koehl MAR, Crimaldi JP, Dombroski DE. 2013 Wind chop and ship wakes determine hydrodynamic stresses on larvae settling on different microhabitats in fouling communities. *Mar. Ecol. Prog. Ser.* **479**, 47–62. (doi:10.3354/meps10193)
28. Reidenbach MA, Koseff JR, Koehl MAR. 2009 Hydrodynamic forces on larvae affect their settlement on coral reefs in turbulent, wave-driven flow. *Limnol. Oceanogr.* **54**, 318–330. (doi:10.4319/lo.2009.54.1.0318)
29. Alldredge AL, Gotschalk C. 1988 In situ settling behavior of marine snow. *Limnol. Oceanogr.* **33**, 339–351. (doi:10.4319/lo.1988.33.3.0339)
30. Finelli CM, Hart DD, Merz R. 2002 Stream insects as passive suspension feeders: effects of velocity and food concentration on feeding performance. *Oecologia* **131**, 145–153. (doi:10.1007/s00442-001-0852-x)
31. Braimah SA. 1987 The influence of water velocity on particle capture by the labral fans of larvae of *Simulium bivittatum* Malloch (Diptera: Simuliidae). *Can. J. Zool* **65**, 2395–2399. (doi:10.1139/z87-360)
32. Hart DD, Finelli CM. 1999 Physical-biological coupling in streams: the pervasive effects of flow on benthic organisms. *Annu. Rev. Ecol. Syst.* **30**, 363–395. (doi:10.1146/annurev.ecolsys.30.1.363)
33. Shimeta J, Starczak VR, Ashiru OM, Zimmer CA. 2001 Influences of benthic boundary-layer flow on feeding rates of ciliates and flagellates at the sediment-water interface. *Limnol. Oceanogr.* **46**, 1709–1719. (doi:10.4319/lo.2001.46.7.1709)
34. Grünbaum D. 1995 A model of feeding currents in encrusting bryozoans shows interference between zooids within a colony. *J. Theor. Biol.* **174**, 409–425. (doi:10.1006/jtbi.1995.0108)
35. Bruus H. 2007 *Theoretical microfluidics*. Oxford, UK: Oxford University Press.
36. Schlichting H, Gersten K. 2000 *Boundary-layer theory*. New York, NY: Springer.
37. Vacchiano EJ, Kut JL, Wyatt ML, Buhse HE. 1991 A novel method for mass-culturing *Vorticella*. *J. Protozool.* **38**, 608–613.
38. Blake JR. 1971 A note on the image system for a stokeslet in a no-slip boundary. *Math. Proc. Camb. Phil. Soc.* **70**, 303–310. (doi:10.1017/S0305004100049902)
39. Blake JR, Chwang AT. 1974 Fundamental singularities of viscous flow. *J. Eng. Math.* **8**, 23–29. (doi:10.1007/BF02353701)
40. Blake JR, Liron N, Aldis GK. 1982 Flow patterns around ciliated microorganisms and in ciliated ducts. *J. Theor. Biol.* **98**, 127–141. (doi:10.1016/0022-5193(82)90062-5)
41. Pepper RE, Roper M, Ryu S, Matsudaira P, Stone HA. 2010 Nearby boundaries create eddies near microscopic filter feeders. *J. R. Soc. Interface* **7**, 851–862. (doi:10.1098/rsif.2009.0419)
42. Helman J, Hesselink L. 1989 Representation and display of vector field topology in fluid flow data sets. *Computer* **22**, 27–36. (doi:10.1109/2.35197)
43. Asadzadeh SS, Nielsen LT, Andersen A, Dölger J, Kiørboe T, Larsen PS, Walther JH. 2019 Hydrodynamic functionality of the lorica in choanoflagellates. *J. R. Soc. Interface* **16**, 20180478. (doi:10.1098/rsif.2018.0478)
44. Pepper RE. 2021 Data from: The effect of external flow on the feeding currents of sessile microorganisms. Dryad Digital Repository. (doi:10.5061/dryad.4j0zpc88m)
45. Sanders RW, Porter KG, Bennett SJ, DeBiase AE. 1989 Seasonal patterns of bacterivory by flagellates, ciliates, rotifers, and cladocerans in a freshwater planktonic community. *Limnol. Oceanogr.* **34**, 673–687. (doi:10.4319/lo.1989.34.4.0673)
46. Carrias JF, Amblard C, Bourdier G. 1996 Protistan bacterivory in an oligomesotrophic lake: importance of attached ciliates and flagellates. *Microb. Ecol.* **31**, 249–268. (doi:10.1007/BF00171570)
47. Nagai M, Oishi M, Oshima M, Asai H, Fujita H. 2009 Three-dimensional two-component velocity measurement of the flow field induced by the *Vorticella picta* microorganism using a confocal microparticle image velocimetry technique. *Biomicrofluidics* **3**, 014105. (doi:10.1063/1.3105106)
48. Cortez R, Varela D. 2015 A general system of images for regularized Stokeslets and other elements near a plane wall. *J. Comput. Phys.* **285**, 41–54. (doi:10.1016/j.jcp.2015.01.019)
49. Kemp PF, Cole JJ, Sherr BF, Sherr EB. 1993 *Handbook of methods in aquatic microbial ecology*. Boca Raton, FL: CRC Press.
50. Weisse T. 2002 The significance of inter- and intraspecific variation in bacterivorous and herbivorous protists. *Antonie Van Leeuwenhoek* **81**, 327–341. (doi:10.1023/A:1020547517255)